



# Deep-learning-based recognition of composite vortex beams through long-distance and moderate-to-strong atmospheric turbulence

Shen Cai , Zhihui Li, Zheqiang Zhong ,\* and Bin Zhang

College of Electronics and Information Engineering, *Sichuan University*, Chengdu, Sichuan 610065, China



(Received 11 December 2023; accepted 24 June 2024; published 12 July 2024)

Orbital angular momentum (OAM), as a physical dimension of light, has been demonstrated to enhance the channel capacity and turbulence resistance of free-space optical (FSO) communication. However, the channel crosstalk in OAM-based FSO communication inevitably increases with transmission distance and turbulence intensity. Here, we propose a deep-learning-based recognition of a composite vortex beam to extend the regime of moderate-to-strong turbulence and long-distance FSO links. The composite vortex beam is generated by a coherent combination of two subbeams carrying different helical charges and phase delays, providing its helical charges and phase delay as new multiplexing dimensions and exhibiting better turbulence resistance compared to a single subbeam. We also developed a modified regular network to achieve the high-accuracy recognition of a composite vortex beam over a long distance at moderate-to-strong atmospheric turbulence. We believe that our approach has potential in deep-learning-based OAM high-capacity communication systems.

DOI: [10.1103/PhysRevA.110.013508](https://doi.org/10.1103/PhysRevA.110.013508)

## I. INTRODUCTION

Free-space optical communication (FSO) can achieve high transmission rates, low latency, and high security through the modulation and demodulation of lasers [1]. Orbital angular momentum (OAM), as a promising degree of freedom for multiplexing data, has been utilized to achieve high-capacity communication in free space [2–5]. However, OAM-based FSO communication inevitably suffers from the issues of atmospheric effects, including diffraction, refraction, atmospheric extinction, pointing errors, and most importantly, turbulence [6–9]. These adverse effects will scramble the wavefronts of OAM modes and destroy the orthogonality between the OAM channels. The deteriorated orthogonality will increase the interchannel fading and crosstalk [10,11]. Consequently, it is challenging to realize OAM-based communication through the atmosphere, especially in long-distance and moderate-to-strong turbulence [12,13].

As a potential approach, a composite vortex beam with more complex spatial structures and degrees of freedom has been proposed [14]. For instance, Huang *et al.* analyzed the antiturbulence performance of a perfect vortex beam [15]. Zhu *et al.* used a beam with three-dimensional information containing a phase delay, helical charge, and radial index [16]. In addition, machine learning methods, such as support vector machines (SVMs) [17], artificial neural network (ANN) [18],  $k$ -nearest neighbors [19], naive Bayes classification [20], and convolutional neural network (CNN) [21,22] have been utilized to enhance the performance of FSO systems. For instance, Zhou *et al.* achieved a recognition of fractional-order helical charges with a resolution of 0.1 and an accuracy of 99.07% in weak turbulence at a transmission distance of

1500 m [23]. Zhang *et al.* achieved the classification of an arbitrary superposition of two OAM modes with random helical charges by training a small sample of images [24]. These previous works are mainly focused on the regime of weak turbulence, suitable for short-range high-rate FSO links [25]. Extending the regime to long-distance and moderate-to-strong turbulence in FSO links is still challenging.

Here, we propose a deep-learning-based recognition of a composite vortex beam to extend the regime to moderate-to-strong turbulence and long-distance FSO links. The composite vortex beam is generated by a coherent combination of two subbeams carrying different helical charges and phase delay, providing its helical charges and phase delay as new multiplexing dimensions and exhibiting better turbulence resistance compared to a single subbeam. Our results indicate that by properly selecting the helical charges and phase delay, the composite vortex beam can achieve high recognition accuracy even with long-distance and moderate-to-strong turbulence.

## II. METHODS

### A. Model of a composite vortex beam

The generation, transmission, and recognition of a composite vortex beam is schematically illustrated in Fig. 1. By the coaxial coherent combination of Laguerre-Gaussian (LG) beams with different OAM modes and phase delays, a composite vortex beam can be obtained, expressed as

$$E_c(r, \theta, z) = \sum_{i,j} E_{p,m_i}(r, \theta, z) + E_{p,m_j}(r, \theta, z) \times \exp(i \Delta \varphi_{i,j}) \quad (i \neq j), \quad (1)$$

where  $\Delta \varphi_{(i,j)}$  is the phase delay between the OAM mode  $m_i$  and  $m_j$ .

\*Contact author: zheqiangzhong@scu.edu.cn

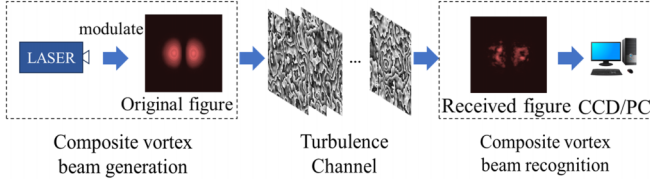


FIG. 1. Schematic illustration of FSO link using a composite vortex beam.

In the composite vortex beam, the helical charges  $m_{(i,j)}$  and phase delay  $\Delta\varphi_{(i,j)}$  can be the multiplexing dimensions, enhancing the channel capacity. Compared to a single subbeam, the composite beam also can exhibit better turbulence resistance, thus providing potential in long-distance and moderate-to-strong turbulence.

Hereafter, we take the composite vortex beam obtained by two LG beams as an example. The LG beam, with zero central light intensity, a helical wavefront, and a relatively simple structure, is expressed as

$$E_{p,m}(r, \theta, z) = \sqrt{\frac{2p!}{\pi(p+|m|)!}} \frac{1}{w(z)} \left[ \frac{r\sqrt{2}}{w(z)} \right]^{|m|} L_p^{|m|} \times \left[ \frac{2r^2}{w^2(z)} \right] \exp\left[ \frac{-r^2}{w^2(z)} \right] \exp(-im\theta) \times \exp\left( \frac{ikr^2z}{2(z^2+z_0^2)} \right) \times \exp\left[ i(2p+|m|+1)\tan^{-1}\left(\frac{z}{z_0}\right) \right], \quad (2)$$

where  $r, \theta, z$  denote the radial distance, azimuth angle, and transmission distance of the beam, respectively.  $w(z)$  denotes the radius of the beam waist, which is given by  $w(z) = w_0\sqrt{1+(z/z_0)^2}$ ,  $w_0$  denotes the beam waist,  $z_0$  denotes the Rayleigh distance,  $z_0 = \pi w_0^2/\lambda$ ,  $\lambda$  denotes the wavelength of the beam, and  $k = 2\pi/\lambda$  denotes the wave number. The term  $(2p+|m|+1)\tan^{-1}(z/z_0)$  denotes the Gouy phase,  $m$  denotes the OAM mode, helical charge, or angular exponent,  $p$  denotes the radial exponent, and  $L_p^{|m|}$  denotes the Laguerre polynomial of the contraction,

$$L_p^{|m|}(x) = (-1)^{|m|} \frac{d^{|m|}}{dx^{|m|}} L_{p+|m|}(x). \quad (3)$$

Consequently, the composite vortex beam can be expressed as

$$E_{m_1, m_2}(r, \theta, z) = E_{p, m_1}(r, \theta, z) + E_{p, m_2}(r, \theta, z) \exp(i\Delta\varphi). \quad (4)$$

According to Eq. (4), the intensity distributions of the composite vortex beam with different OAM modes and phase delays are illustrated in Fig. 2. In Figs. 2(a)–2(d), the composite vortex beam, generated by the superposition of an OAM beam with  $m_1 = -1, m_2 = 1$ , exhibits two petals and is rotated clockwise by  $\pi/4$ . Similarly, in Figs. 2(e)–2(h), the composite vortex beam, generated by the superposition of an OAM beam with  $m_1 = -1, m_2 = +2$ , and a phase delay of  $\Delta\varphi = \pi/2$ , has three petals and is rotated clockwise by  $\pi/6$ .

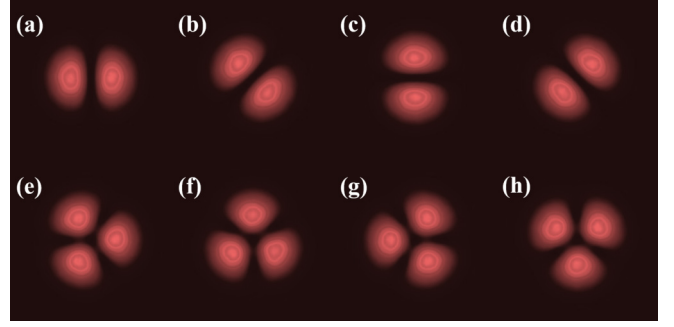


FIG. 2. Composite vortex beams: (a)–(d)  $m_1 = -m_2 = 1$ , (e)–(h)  $m_1 = -1, m_2 = +2$ . The parameters are wavelength  $\lambda = 632.8$  nm, beam waist  $w_0 = 15$  cm, and radial index  $p = 0$ .

In Fig. 2, it can be concluded that by changing the phase delay of the LG beams, the composite vortex beam will rotate  $\Delta\varphi/|m_1 - m_2|$  clockwise ( $\Delta\varphi > 0$ ) or anticlockwise ( $\Delta\varphi < 0$ ). The rotation angle is dependent on both the phase delay and the OAM modes. The recognition of such composite vortex beam can be achieved by identifying the number of petals, and the phase delay can be obtained by the pattern recognition of the composite vortex beam. However, previous works have primarily focused on identifying the helical charge of the vortex beam, but not the pattern recognition of a composite vortex beam.

## B. Propagation of a composite vortex beam through atmosphere

The transmission of light in the atmosphere can be numerically calculated using multilayer random phase screens. The power spectrum inversion method based on fast Fourier transform is used for generating the random phase screen, based on the von Kármán spectrum [26], expressed as

$$\Phi_n(\kappa) = 0.033C_n^2 \frac{\exp(-\kappa^2/\kappa_m^2)}{(\kappa^2 + \kappa_0^2)^{11/6}}, \quad (5)$$

where  $0 \leq \kappa < \infty$ ,  $\kappa_0 = 2\pi/L_0$ ,  $\kappa_m = 5.92/l_0$ .

The phase spectrum is obtained by the Markov approximation, expressed as

$$\Phi(\kappa_x, \kappa_y, z) = 2\pi k^2 \Delta z \Phi_n(\kappa_x, \kappa_y, z), \quad (6)$$

where  $k = 2\pi/\lambda$  is the wave number, and  $\lambda$  is the wavelength. In Eq. (5),  $\Delta z$  is the propagation distance between sequential phase screens.

Then, the phase screen  $P(x, y)$  can be written as

$$P(x, y) = \text{IFFT}[a_R \sqrt{\Phi(\kappa_x, \kappa_y, z)}], \quad (7)$$

where IFFT is the inverse two-dimensional (2D) Fourier transform, and  $a_R$  is a complex uniform random matrix.

In this paper, the parameters for atmospheric turbulence are as follows: The propagation distance is  $z = 10$  km, the interval distance is  $\Delta z = 200$  m, the outer scale is  $L_0 = 10$  m, and the inner scale is  $l_0 = 0.005$  m. The refractive index structure constants  $C_n^2$  are set to  $1 \times 10^{-15} \text{ m}^{-2/3}$ ,  $1 \times 10^{-14} \text{ m}^{-2/3}$ , and  $1 \times 10^{-13} \text{ m}^{-2/3}$  for weak, moderate, and strong turbulence, respectively.

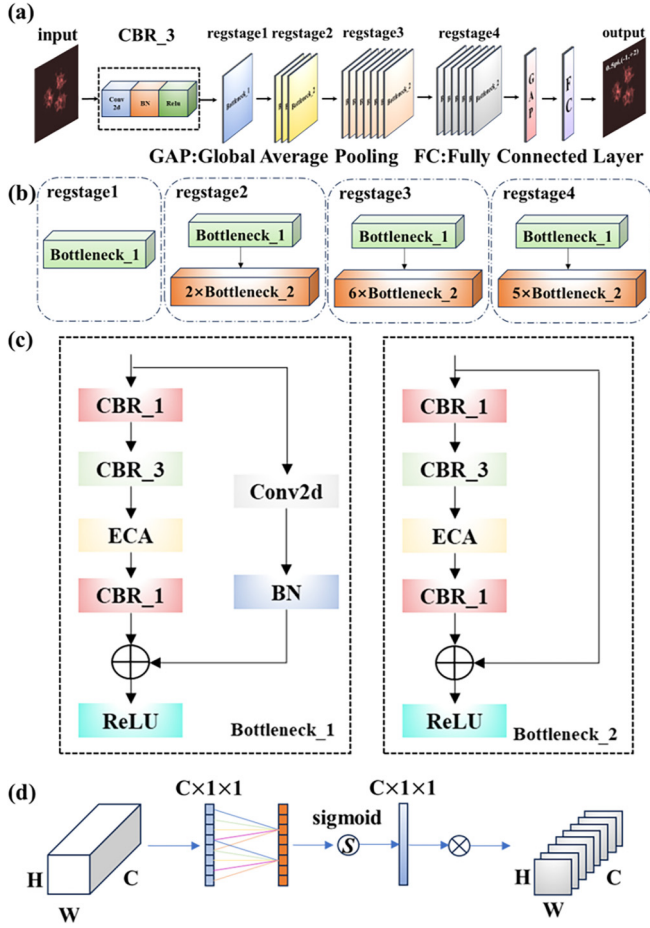


FIG. 3. Neural network structure of the modified RegNet-based network. (a) Main structure of the proposed RegNet-based network. (b) Structural diagram of each RegStage. (c) Structural diagram of Bottleneck. (d) Structural diagram of ECA.

**C. Modified RegNet-based network**

Herein, to achieve the recognition of composite vortex beam through long-distance and moderate-to-strong turbulence, we have employed a modified regular network (RegNet)-based network [27]. The network primarily involves adjusting the model distribution by modifying the parameters to derive varied network structures for addressing diverse classification tasks. The key parameters include the number of blocks in each RegStage  $d_i$ , the number of channels in the output matrix of each RegStage  $w_i$ , and the width of each Group in the block  $g$ . By adjusting these parameters, network performance can be optimized, and the number of parameters in the model can be significantly reduced to accelerate the training speed. In this paper, a modified RegNet-based network is proposed for the recognition of composite vortex beam, with the model framework illustrated in Fig. 3.

In the modified RegNet-based network, the image is first input into the CBR<sub>3</sub> module for feature extraction, consisting of Conv2d convolution, batch normalization (BN), and ReLU activation function, denoted as the CBR<sub>x</sub> module in Fig. 3(a), where x represents the size of the convolution kernel. Subsequently, the feature map is fed into the Body consisting of four RegStages as depicted in Fig. 3(b), each

containing a Bottleneck<sub>x</sub> structure resembling Fig. 3(c). The distinction between Bottleneck<sub>1</sub> and Bottleneck<sub>2</sub> lies in the addition of a Conv2d layer and a BN layer on the shortcut branch in Bottleneck<sub>1</sub>. Finally, for classification and to avoid overfitting, the output of the body is fed into the global average pooling and fully connected layer.

Compared with the original RegNet, the modified RegNet-based network primarily enhances the grouped convolution residual structure within each Block in RegStage, and integrates the Efficient Channel Attention (ECA) module after the grouped convolution [28]. This further focuses on the feature distribution of the image and improves the feature extraction ability of the model. The structure of the ECA model, illustrated in Fig. 3(d), is an effective channel attention mechanism using a local cross-channel interaction strategy without dimensionality reduction. This approach conserves parameters during cross-channel interactions and simultaneously avoids channel cuts.

**III. RESULTS AND DISCUSSION**

Compared to a single vortex beam, the composite vortex beam can provide more multiplexing dimensions and exhibit better turbulence resistance. However, the proper selection of OAM modes and phase delay is of importance. In this work, to evaluate the performance of the modified RegNet-based network on identifying the composite vortex beam, we generate a data set corresponding to 80 classifications of a composite beam consisting of nine OAM modes and multiple phase delay, by fixing the helical charge of one of the beams ( $m_1 = -1$ ) and adjusting the helical charge and the phase delay of the other beam. In addition, in order to expand the channel capacity while achieving a high recognition, we evenly selected the phase delay for different combinations of OAM modes. According to Fig. 2, the maximum rotation angle  $\phi_{max}$ , denoting the angle between each petal, is expressed as

$$\phi_{max} = \frac{2\pi}{|m_2 - m_1|}, \tag{8}$$

where  $m_1$  and  $m_2$  are the helical charge of beams.

We can easily find that the maximum rotation angle  $\phi_{max}$  decreases with increasing OAM mode, so that the rotation angular interval  $\phi$  should decrease corresponding to the OAM mode to maintain its high recognition. The rotation angular interval  $\phi$  is defined as

$$\Delta\phi = \frac{\phi_{max}}{N}, \tag{9}$$

where  $N$  is the channel number for each combination of OAM modes.

According to the relationship between angle and phase, we can calculate the phase delay interval, expressed as

$$\Delta\varphi = \frac{2\pi}{N} = \Delta\phi|m_2 - m_1|. \tag{10}$$

Equations (8)–(10) show a complete relationship between the phase delay interval as well as the rotation angle. We can know that both of them can be changed by changing the combination of the number of channels and the number of topological charges.

TABLE I. Combinations of OAM modes and corresponding channel number and phase delay interval.

Combinations	Channel number	Phase delay interval
(-1, +1)	32	$\frac{\pi}{16}$
(-1, +2)	16	$\frac{\pi}{8}$
(-1, +3)	8	$\frac{\pi}{4}$
(-1, +4)	8	$\frac{\pi}{4}$
(-1, +5)	8	$\frac{\pi}{4}$
(-1, +6)	4	$\frac{\pi}{2}$
(-1, +7)	2	$\pi$
(-1, +8)	2	$\pi$

As the phase interval decreases, for a specific combination of helical charges, the number of channels increases, leading to a reduction in the angular interval. This suggests that the differences between the images become smaller, facing a greater challenge for the neural network in terms of identification. After many attempts and training, we have selected the combination of OAM modes and corresponding channel number given in Table I for an example. Figure 4 also gives the maximum rotation angles and the rotation angular interval corresponding to each combination of OAM modes.

From Fig. 4 and Table I, it can be seen that both the maximum rotation angle and the phase delay interval decrease with an increase of OAM modes, while the rotation angle interval tends to increase with an increase of the selected channel number, indicating the importance of choosing a proper channel number. This is because the maximum rotation angle of the combination of large OAM modes is very small, and the neighboring petals within the rotating beam are very close to one another. Under strong atmospheric turbulence, the petals are easily twisted and destroyed, and may interfere with each other, making it impossible to maintain high recognition accuracy.

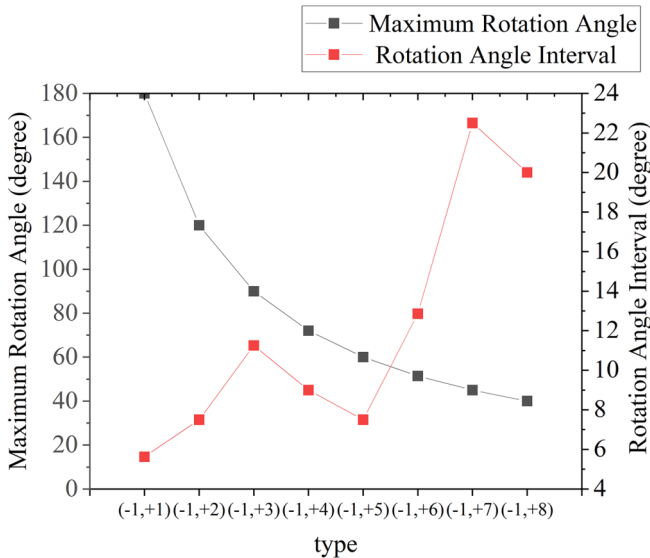


FIG. 4. Maximum rotation angle and rotation angular interval for each combination of OAM modes.

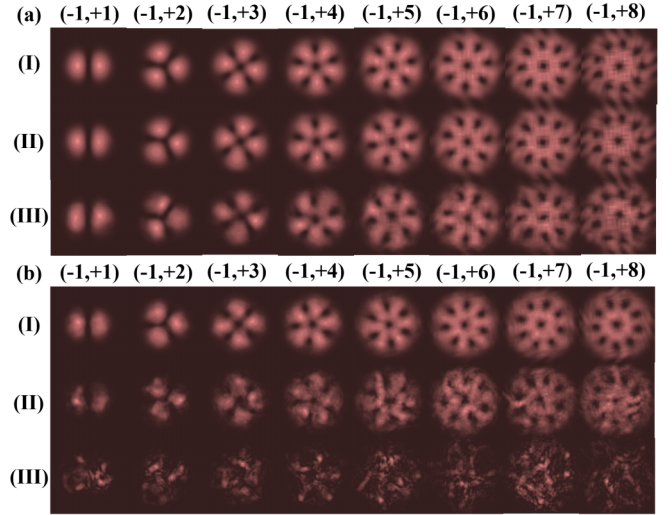


FIG. 5. Degraded images in simulations with different helical charge combinations, from (I) to (III) for weak, moderate, and strong turbulence, respectively. (a) Beam waist  $w_0 = 0.03$  m, propagation distance  $z = 1$  km. (b) Beam waist  $w_0 = 0.15$  m, propagation distance  $z = 10$  km.

### A. Simulation results and analysis

The simulation generates 34 000 degraded images across 80 classifications, in which the training set and the test set are divided in an 8:2 ratio, containing three kinds of turbulence strengths, weak ( $1 \times 10^{-15} \text{ m}^{-2/3}$ ), moderate ( $1 \times 10^{-14} \text{ m}^{-2/3}$ ), and strong ( $1 \times 10^{-13} \text{ m}^{-2/3}$ ). To optimize the performance of the network under moderate-to-strong turbulence, the data set includes images at weak, moderate, and strong turbulence in a ratio of 1:2:5. The degraded images with diverse helical charge combinations with different, through weak, moderate, and strong turbulence, are shown in Fig. 5.

From Fig. 5(a), it can be found that the degradation of the images in (I)–(III) increases with an increase of turbulence intensity, but the degraded images can still be distinguished. On the contrary, Fig. 5(b) shows the simulation results of laser beams with a propagation distance of 10 km. Compared with Fig. 5(a), the degradation in Fig. 5(b)(II) propagated under long-distance and moderate turbulence is more serious. In addition, the degraded image in Fig. 5(b)(III) propagated by strong turbulence over a long distance has been severely distorted.

In order to accurately evaluate the recognition performance of the modified RegNet-based network, we used the recognition accuracy, expressed as

$$\text{accuracy} = \frac{\sum_{n=1}^N f(n)}{N} \times 100\%, \quad (11)$$

$$f(n) = \begin{cases} 1, & l_n = l_n^*, \\ 0, & l_n \neq l_n^*, \end{cases} \quad (12)$$

where  $l_n$  is the real label corresponding to the degraded LG beam image,  $l_n^*$  denotes the classification label predicted by the network, and  $n$  is the label number. We first trained the data set in Fig. 5(a) under different turbulence at a short distance of 1 km, and then we found the recognition efficiency quickly



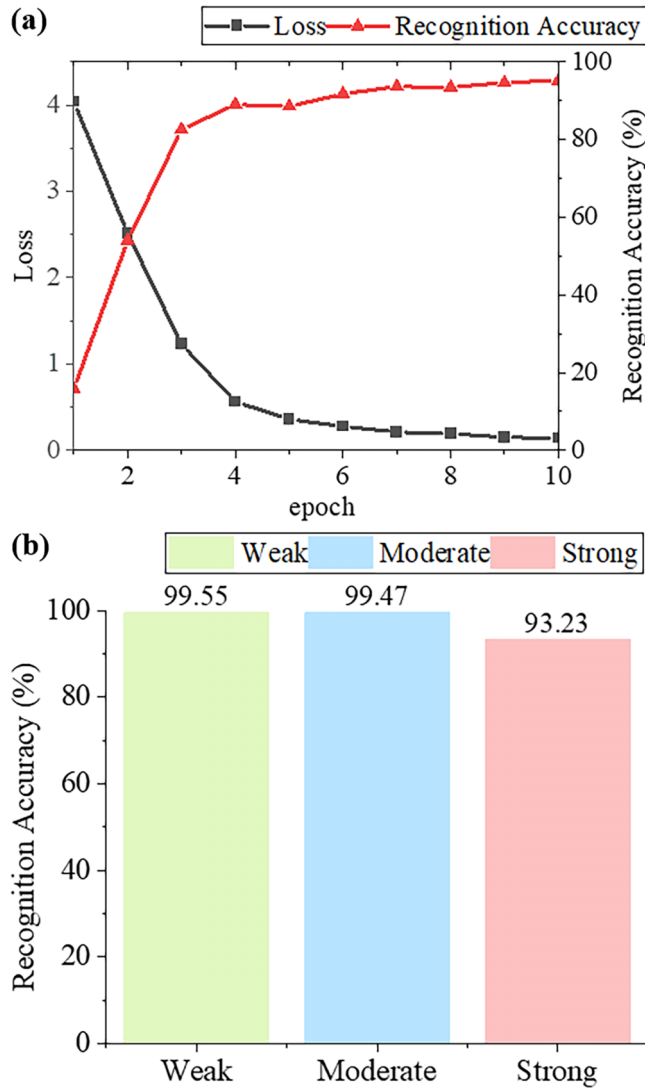


FIG. 6. Schematic diagram of simulation results. (a) Schematic diagram of the loss function and recognition accuracy while training. (b) Recognition accuracy of propagation in turbulence channel with different turbulence intensities.

reaches 100% after 3 epochs, which initially proved that our proposed neural network structure and classification method are effective. Later, we trained the network using the data in Fig. 5(b) under different turbulence at a short distance of 10 km to further demonstrate the feasibility of our approach, and the training results are shown in Fig. 6.

In Fig. 6(a), both the loss function values and the accuracy on the validation set after 10 epochs of network iterations are shown. Subsequently, we explored the relationship between the accuracy of OAM recognition and turbulence intensity in Fig. 6(b). Our investigation revealed that the recognition accuracy can reach approximately 100% in both weak and moderate turbulence intensities, while achieving 93.23% in strong turbulence. As turbulence intensity increases, recognition accuracy decreases to a certain extent, attributed to the severe deformation and fragmentation of the composite vortex beam under strong turbulence, making adequate feature extraction challenging for the neural network.

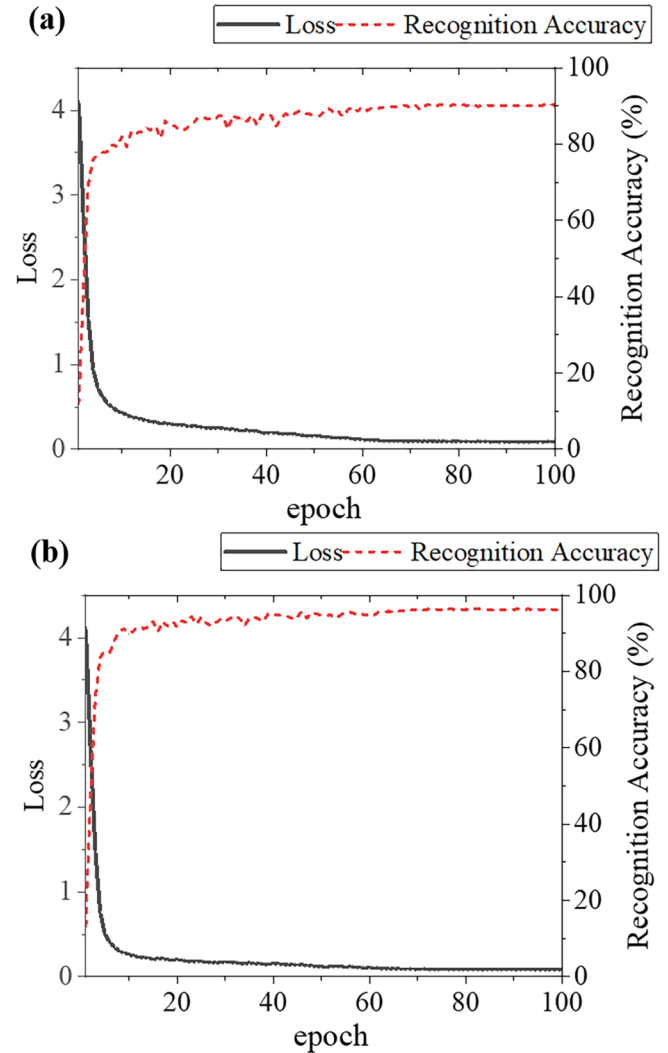


FIG. 7. Schematic diagram of the loss function and recognition accuracy while training. Transmission distance  $z = 10$  km, (a) beam waist size  $w_0 = 0.12$  m, and (b) beam waist size  $w_0 = 0.18$  m.

Since the size of the beam waist affects the divergence angle, it also affects the result of beam degradation and the recognition result of the network considering the practical effects. In order to verify the recognition capability of our network structure under different sizes of beam waist, we set the beam waist size  $w_0$  to 0.12 and 0.18 m in addition to  $w_0 = 0.15$  m. The training results are presented in Fig. 7.

Under the same training set structure, the recognition accuracy reaches 90.3% and 96.5%, respectively, in Figs. 7(a) and 7(b). This indicates that our network is suitable for composite LG beam recognition under different practical conditions.

It is noteworthy that despite training our neural network for long distances and in moderate-to-strong turbulence, our model performs well, as demonstrated in Table II.

Table II shows a comparison of recent works and our work. It is noteworthy that Ref. [23] and our work achieved a similar recognition accuracy under a turbulence intensity of  $1 \times 10^{-15} \text{ m}^{-2/3}$ . Moreover, Refs. [30,31] were both tested under a turbulence intensity of  $1 \times 10^{-14} \text{ m}^{-2/3}$ , while Ref. [31] is

TABLE II. Comparison of recent works and our work.

Reference	Distance	Turbulence intensity	Mode amount	Recognition accuracy
[23]	1500 m	$1 \times 10^{-15} \text{ m}^{-2/3}$	10	99.07%
[29]	1000 m	$1 \times 10^{-14} \text{ m}^{-2/3}$	30	85.83%
[30]	2000 m	$1 \times 10^{-14} \text{ m}^{-2/3}$	16	87.73%
[31]	1500 m	Up to $5 \times 10^{-14} \text{ m}^{-2/3}$	10	85.30%
This work	10000 m	$1 \times 10^{-15} \text{ m}^{-2/3}$	80	99.55%
		$1 \times 10^{-14} \text{ m}^{-2/3}$		99.47%
		$1 \times 10^{-13} \text{ m}^{-2/3}$		93.23%

tested with a transmission distance of 2000 m, and the maximum turbulence intensity of Ref. [32] is  $5 \times 10^{-14} \text{ m}^{-2/3}$ . Consequently, our work demonstrates the ability to enhance channel capacity and achieve high recognition rates even over long distances and in moderate-to-strong turbulence. This enhancement can be attributed to two factors: the construction of an appropriate data set, which involved optimization of helical charges and rotation angle, and the use of a modified RegNet.

Furthermore, we investigated the difference in recognition accuracy between different classifications of the images shown in Fig. 8.

According to Fig. 8, we attribute the superior recognition accuracy of our model to our pattern classification method, which leverages two distinct features: rotation angle and helical charge. The significant differences in characteristics between each helical charge combination contribute to the effectiveness of our approach. Each composite beam exhibits a unique intensity distribution, enabling our CNN-trained neural network model to maintain accurate classification even when the light intensity distribution is disrupted by strong turbulence. Consequently, in future work, we aim to further reduce the angular spacing of the dual-mode beams, allowing for the utilization of each helical charge combination.

### B. Experimental results and analysis

The diagram of the experimental setup is shown in Fig. 9(a). In our experimental setup, using the method in

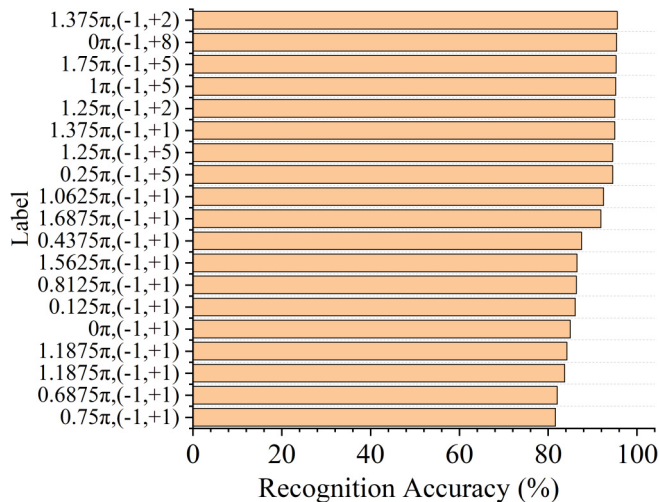


FIG. 8. Representative classifications and corresponding recognition accuracy.

Ref. [32], we initially generate the original images corresponding to 80 composite vortex beams. Subsequently, we employed the Gerchberg-Saxton (GS) algorithm to generate the Fresnel holograms. The Gaussian laser beam exits through the polarizer and small aperture diaphragm and then passes through the beam expander mirror before going to  $\text{SLM}_1$  to be modulated by an OAM hologram, and after that it passes

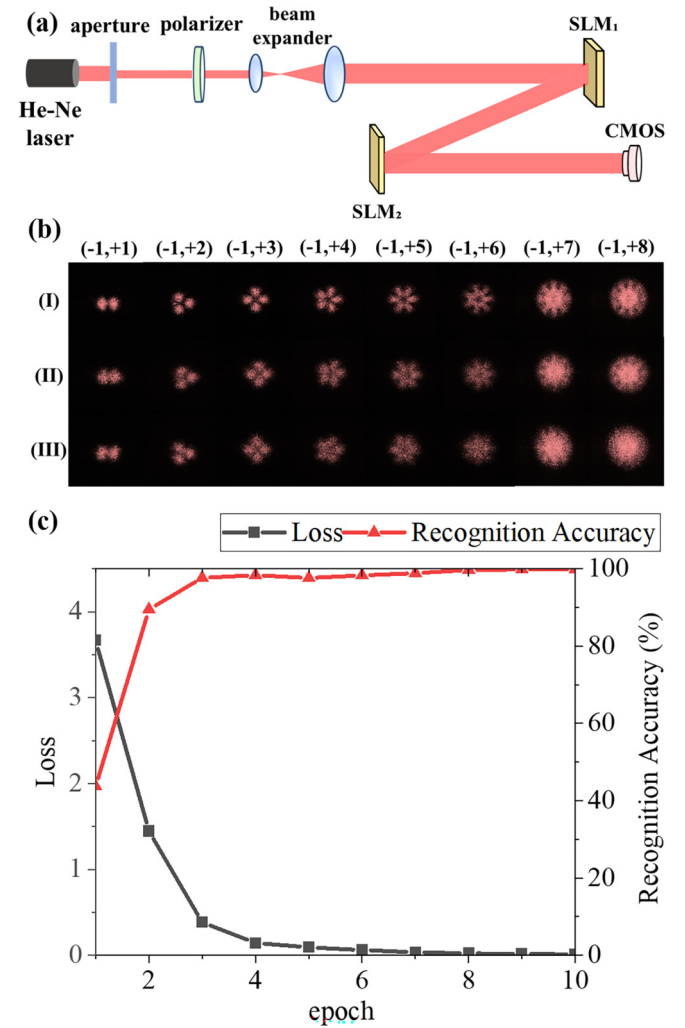


FIG. 9. (a) Schematic diagram of the experimental setup. SLM: spatial light modulator. CMOS: complementary metal-oxide semiconductor. (b) Degraded experimental images with different helical charge combinations, from (I) to (III) for weak, moderate, and strong turbulence, respectively. (c) Schematic diagram of the loss function and recognition accuracy.

through the phase screen loaded on SLM<sub>2</sub> and receives the image at the CMOS camera.

In order to simulate a realistic atmospheric transport environment, a set of phase screens consisting of three different turbulence intensities were generated from Eqs. (5)–(7) in this study. The experimental parameters are set as follows: Both the SLMs' resolutions are  $N_x \times N_y = 1272 \times 1024$ , wavelength  $\lambda = 632.8$  nm, inner scale  $l_0 = 0.005$  m, outer scale  $L_0 = 10$  m, and turbulence screen interval  $\Delta z = 1000$  m. With different modes of holograms, we loaded different turbulence screen images and constructed the data set by capturing the images at the CMOS.

As in Fig. 5, we can see that for moderate and strong turbulence in Figs. 9(b)(II) and 9(b)(III), there is some degree of degradation compared to the weak turbulence in Fig. 9(b)(I), and the degradation in Fig. 9(b)(III) is more severe under strong turbulence than the degraded image under moderate turbulence in Fig. 9(b)(II).

In total, a total of 16 000 images were captured at the CMOS under different turbulence intensities using holograms of 80 OAMs, out of which 3200 images were used as the test set and the remaining 12 800 images were used as the training set. A total of 10 epochs of training were carried out with a total time of 1590 s, and the relationship between the loss function and the accuracy on the validation set is shown in Fig. 9(c).

From Fig. 9(c), we can find that the recognition accuracy reaches 100%, which is the same as our simulated data set, and this demonstrates the correctness of our classification method.

#### IV. CONCLUSION

In conclusion, we have proposed the deep-learning-based recognition of a composite vortex beam through long-distance and moderate-to-strong turbulence. Our approach involves the simultaneous recognition of helical charges and the phase delay of the composite vortex beam. To maintain high recognition accuracy, the OAM modes and phase delay have been carefully selected, and the data set is also specifically designed. In the simulation, we achieved a recognition accuracy of 93.23% for different OAM modes through a 10 km distance of moderate-to-strong turbulence. Furthermore, experimental results confirmed the method's effectiveness, with a recognition accuracy of 100% over a strong turbulence channel. Both the simulation and experiment demonstrate that by appropriately choosing the helical charge and phase delay, the composite vortex beam can maintain high recognition accuracy over long distances and under moderate-to-strong turbulence. We believe that our approach has the potential to be applied in next-generation, deep-learning-based OAM high-capacity communication systems.

- 
- [1] F. P. Guiomar, M. A. Fernandes, J. L. Nascimento, V. Rodrigues, and P. P. Monteiro, Coherent free-space optical communications: Opportunities and challenges, *J. Lightwave Technol.* **40**, 3173 (2022).
  - [2] A. E. Willner, K. Pang, H. Song, K. Zou, and H. Zhou, Orbital angular momentum of light for communications, *Appl. Phys. Rev.* **8**, 041312 (2021).
  - [3] J. Wang, J. Liu, S. Li, Y. Zhao, J. Du, and L. Zhu, Orbital angular momentum and beyond in free-space optical communications, *Nanophotonics* **11**, 645 (2022).
  - [4] Z. Wan, H. Wang, Q. Liu, X. Fu, and Y. Shen, Ultra-degree-of-freedom structured light for ultracapacity information carriers, *ACS Photonics* **10**, 2149 (2023).
  - [5] A. E. Willner, H. Huang, Y. Yan, Y. Ren, N. Ahmed, G. Xie, C. Bao, L. Li, Y. Cao, Z. Zhao *et al.*, Optical communications using orbital angular momentum beams, *Adv. Opt. Photonics* **7**, 66 (2015).
  - [6] L. Zhang, X. Tian, Y. Jiang, X. Li, Z. Li, D. Li, and S. Zhang, Adversarial network for multi-input image restoration under strong turbulence, *Opt. Express* **31**, 41518 (2023).
  - [7] Z. Zhu, M. Janasik, A. Fyffe, D. Hay, Y. Zhou, B. Kantor, T. Winder, R. W. Boyd, G. Leuchs, and Z. Shi, Compensation-free high-dimensional free-space optical communication using turbulence-resilient vector beams, *Nat. Commun.* **12**, 1666 (2021).
  - [8] S. Fu and C. Gao, Influences of atmospheric turbulence effects on the orbital angular momentum spectra of vortex beams, *Photonics Res.* **4**, B1 (2016).
  - [9] H. E. Nistazakis, T. A. Tsiftsis, and G. S. Tombras, Performance analysis of free-space optical communication systems over atmospheric turbulence channels, *IET Commun.* **3**, 1402 (2009).
  - [10] G. A. Tyler and R. W. Boyd, Influence of atmospheric turbulence on the propagation of quantum states of light carrying orbital angular momentum, *Opt. Lett.* **34**, 142 (2009).
  - [11] J. A. Anguita, M. A. Neifeld, and B. V. Vasic, Turbulence-induced channel crosstalk in an orbital angular momentum-multiplexed free-space optical link, *Appl. Opt.* **47**, 2414 (2008).
  - [12] A. E. Willner, Y. Ren, G. Xie, Y. Yan, L. Li, Z. Zhao, J. Wang, M. Tur, A. F. Molisch, and S. Ashrafi, Recent advances in high-capacity free-space optical and radio-frequency communications using orbital angular momentum multiplexing, *Philos. Trans. R. Soc. A* **375**, 20150439 (2017).
  - [13] S. Ashrafi, Experimental characterization of a 400 Gbit/s orbital angular momentum multiplexed free-space optical link over 120-meters, *Opt. Lett.* **41**, 622 (2016).
  - [14] C. Huang, L. Bai, J. Li, and Y. Wang, Beam spreading and scintillation of perfect vortex beam propagating in atmospheric turbulence, *Proc. SPIE* **12478**, 582 (2022).
  - [15] J. Zhu, M. Fan, Y. Pu, H. Li, and S. Wang, 1024-ary composite OAM shift keying for free-space optical communication system decoded by a two-step neural network, *Opt. Lett.* **48**, 2692 (2023).
  - [16] L. Liu, Y. Gao, and X. Liu, High-dimensional vortex beam encoding/decoding for high-speed free-space optical communication, *Opt. Commun.* **452**, 40 (2019).
  - [17] S. Wang, X. Guo, Y. Tie, I. Lee, L. Qi, and L. Guan, Graph-based safe support vector machine for multiple classes, *IEEE Access* **6**, 28097 (2018).
  - [18] M. Krenn, R. Fickler, M. Fink, J. Handsteiner, M. Malik, T. Scheidl, R. Ursin, and A. Zeilinger, Communication with

- spatially modulated light through turbulent air across Vienna, *New J. Phys.* **16**, 113028 (2014).
- [19] D. Wang, M. Zhang, M. Fu, Z. Cai, Z. Li, H. Han, Y. Cui, and B. Luo, Nonlinearity mitigation using a machine learning detector based on  $k$ -nearest neighbors, *IEEE Photonics Technol. Lett.* **28**, 2102 (2016).
- [20] S. Zhou, R. Gao, Q. Zhang, H. Chang, X. Xin, Y. Zhao, J. Liu, and Z. Lin, Data-defined naïve Bayes (DNB) based decision scheme for the nonlinear mitigation for OAM mode division multiplexed optical fiber communication, *Opt. Express* **29**, 5901 (2021).
- [21] Z. Mao, H. Yu, M. Xia, S. Pan, D. Wu, Y. Yin, Y. Xia, and J. Yin, Broad bandwidth and highly efficient recognition of optical vortex modes achieved by the neural-network approach, *Phys. Rev. Appl.* **13**, 034063 (2020).
- [22] J. Li, M. Zhang, D. Wang, S. Wu, and Y. Zhan, Joint atmospheric turbulence detection and adaptive demodulation technique using the CNN for the OAM-FSO communication, *Opt. Express* **26**, 10494 (2018).
- [23] J. Zhou, Y. Yin, J. Tang, C. Ling, M. Cao, L. Cao, G. Liu, J. Yin, and Y. Xia, Recognition of high-resolution optical vortex modes with deep residual learning, *Phys. Rev. A* **106**, 013519 (2022).
- [24] L.-F. Zhang, Y.-Y. Lin, Z.-Y. She, Z.-H. Huang, J.-Z. Li, X. Luo, H. Yan, W. Huang, D.-W. Zhang, and S.-L. Zhu, Recognition of orbital-angular-momentum modes with different topological charges and their unknown superpositions via machine learning, *Phys. Rev. A* **104**, 053525 (2021).
- [25] H. Kaushal and G. Kaddoum, Optical communication in space: Challenges and mitigation techniques, *IEEE Commun. Surveys & Tutorials* **19**, 57 (2016).
- [26] T. Von Karman, Progress in the statistical theory of turbulence, *Proc. Natl. Acad. Sci. USA* **34**, 530 (1948).
- [27] I. Radosavovic, R. P. Kosaraju, R. Girshick, K. He, and P. Dollár, Designing network design spaces, in *Proceedings of the IEEE/CVF Conference on Computer Vision and Pattern Recognition* (IEEE, New York, 2020), pp. 10428–10436.
- [28] Q. Wang, B. Wu, P. Zhu, P. Li, W. Zuo, and Q. Hu, ECA-Net: Efficient channel attention for deep convolutional neural networks, in *Proceedings of the IEEE/CVF Conference on Computer Vision and Pattern Recognition* (Ref. [27]), pp. 11534–11542.
- [29] J. Wang, C. Wang, Z. Tan, X. Wang, S. Lei, P. Wu, and C. Yang, Detection of orbital angular momentum carried high-order radial vortex beams using CNN-OAM mode classifier, *Opt. Laser Technol.* **169**, 110027 (2024).
- [30] L. Zhao, Y. Hao, L. Chen, W. Liu, M. Jin, Y. Wu, J. Tao, K. Jie, and H. Liu, High-accuracy mode recognition method in orbital angular momentum optical communication system, *Chin. Opt. Lett.* **20**, 020601 (2022).
- [31] M. Cao, Y. Yin, J. Zhou, J. Tang, L. Cao, Y. Xia, and J. Yin, Machine learning based accurate recognition of fractional optical vortex modes in atmospheric environment, *Appl. Phys. Lett.* **119**, 141103 (2021).
- [32] D. P. Kingma and J. Ba, Adam: A method for stochastic optimization, [arXiv:1412.6980](https://arxiv.org/abs/1412.6980).